



Adsorption of diuron and dichlobenil on multiwalled carbon nanotubes as affected by lead

Guang-Cai Chen^{a,b}, Xiao-Quan Shan^{b,*}, Zhi-Guo Pei^b, Huanhua Wang^b,
Li-Rong Zheng^c, Jing Zhang^c, Ya-Ning Xie^c

^a Research Institute of Subtropical Forestry, Chinese Academy of Forestry, Fuyang, Zhejiang 311400, China

^b State Key Laboratory of Environmental Chemistry and Ecotoxicology, Research Center for Eco-Environmental Sciences, Chinese Academy of Sciences, Beijing 100085, China

^c Beijing Synchrotron Radiation Laboratory, Institute of High Energy Physics, Chinese Academy of Sciences, Beijing 100049, China

ARTICLE INFO

Article history:

Received 15 September 2010

Received in revised form 19 January 2011

Accepted 21 January 2011

Available online 31 January 2011

Keywords:

Diuron

Dichlobenil

Lead

Carbon nanotubes

Adsorption

ABSTRACT

The effect of lead on the adsorption of diuron and dichlobenil on multiwalled carbon nanotubes (MWCNTs) was investigated to explore the possible application of MWCNTs for removal of both herbicides from contaminated water. The adsorption of diuron and dichlobenil on MWCNTs at pH 6 was nonlinear and fit the Polanyi–Manes model well. The adsorption of diuron and dichlobenil was closely correlated with specific surface areas and micropore volumes of MWCNTs. An increase in oxygen content of MWCNTs with same diameters and similar surface areas decreased the adsorption of diuron and dichlobenil, while increased the adsorption of lead. Micro-Fourier transform infrared spectroscopic study indicated that hydrogen bonding is a main mechanism responsible for the adsorption of diuron or dichlobenil onto MWCNTs–O. Oxygen containing groups, mainly carboxylic groups, significantly increased the adsorption of lead through the formations of outer-sphere and inner-sphere complexes, which are verified by X-ray absorption spectroscopic measurements. Oxygen containing groups and the presence of lead diminished the adsorption of diuron and dichlobenil. The suppression mechanisms of lead were ascribed to hydration and complexation of lead with carboxylic groups, which may occupy part of surface of MWCNTs–O. The large hydration shell of lead cations may intrude or shield hydrophobic and hydrophilic sites, resulting in a decreased adsorption of diuron and dichlobenil at the lead-complexed moieties.

© 2011 Elsevier B.V. All rights reserved.

1. Introduction

Diuron is a non-selective herbicide and mainly used for both pre-emergent and post-emergent weed control on broadleaf and grassy weeds along with mosses and algae on crop or non-crop sites [1]. Dichlobenil is used to kill unwanted weeds and is remarkably persistent in soil [2]. Diuron and dichlobenil are frequently detected in ground and surface waters due to their worldwide use, relatively high chemical stability in soils and aquifers, and high leaching potential [3–5]. Lead is common detected metal in natural waters and soils due to discharge of industrial processes and sewage irrigation [6]. There has been increasing concern and more stringent regulation standards pertaining to the application of herbicide and discharge of heavy metals to the aquatic environment [7]. Hence, simultaneous removal of these toxic contaminants from wastewater

is an important environmental issue. Adsorption has been found to be superior to other techniques for wastewater treatment due to its low-cost, high efficient and easy of operation.

Carbon nanotubes (CNTs) have been increasingly applied in the environmental protection as novel materials due to their strong adsorption affinity for both heavy metals and organic chemicals [8–15]. CNTs are considered a superior adsorbent for potential environmental remediation due to their large surface area and high reactivity [16–19]. The sorption mechanisms of organic chemicals by CNTs include hydrophobic interactions [20–23], π – π interaction [24,25], hydrogen bond [26–28], electrostatic interactions and Lewis acid–base interaction [26,29]. However, the relative contribution of a given mechanism to the overall sorption is largely unclear, which needs to be further addressed.

Extensive researches suggested that CNTs have strong sorption affinity for heavy metals due to high chemisorption capability [9,11,30]. It was reported that CNTs show exceptional high adsorption efficiency for lead. The adsorption is significantly influenced by pH of solution and nanotube surface status, which can be controlled by their treatment processes [8]. Further research [30] suggested that oxygen functional groups play an important role

* Corresponding author at: State Key Laboratory of Environmental Chemistry and Ecotoxicology, Research Center for Eco-Environmental Sciences, Chinese Academy of Sciences, Beijing 10085, China. Tel.: +86 10 62923560; fax: +86 10 62923563.

E-mail address: xiaoquan@rcees.ac.cn (X.-Q. Shan).

in lead adsorption to form chemical complex adsorption, which accounts for 75.3% of all lead adsorption capacity [30].

To date, most current studies focus on the adsorption of single organic chemical(s) or heavy metal(s) by CNTs separately. However, the single-solute systems may not represent many systems commonly encountered in the environment, where multiple contaminants may coexist at many contaminated sites [31]. Previous studies suggested that metal cations may influence the environmental fate of toxic chemicals in soil–water systems [32,33]. Our primary study showed that metallic cations may influence the adsorption of atrazine and 2,4,6-trichlorophenol onto CNTs [28,34], implying that organic chemicals exhibit different environmental behaviors in multiple contaminant system from that in single-solute systems.

The coexistence of diuron, dichlobenil and lead tend to influence their adsorption, transport and fate in the environment. However, question on the effects of lead on the adsorption of diuron and dichlobenil or vice versa by MWCNTs have not been addressed. The possible influence should be considered when CNTs were applied as adsorbents in waste water treatment. For these reasons a better understanding of interactions between diuron, dichlobenil and lead during their adsorption on CNTs is becoming an environmentally important issue.

The aims of this study were (i) to elucidate the effect of lead on the adsorption of diuron and dichlobenil on MWCNTs containing oxygen functional groups; and (ii) to provide an insight to the relevant mechanisms using Fourier transform infrared micro-spectroscopic (μ -FTIR) and X-ray absorption spectroscopic (XAS) studies.

2. Materials and methods

2.1. Chemicals

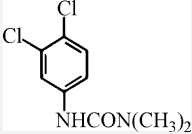
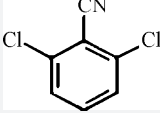
Diuron and dichlobenil were purchased from Sigma–Aldrich Chemical Co. with a reported purity of HPLC-Grade 97.4% and used as received. The selected physiochemical properties are listed in Table 1. $\text{Pb}(\text{NO}_3)_2$ is of guarantee reagent grade. Other chemicals are of analytical reagent grade or better.

2.2. MWCNTs

MWCNTs were purchased from Chengdu Organic Chemistry Co. Ltd., Chinese Academy of Sciences. These MWCNTs were synthesized from ethylene/nitrogen ($\text{C}_2\text{H}_4/\text{N}_2 = 3/2$) mixture by chemical vapor deposition at 823 K using $\text{Fe}/\text{Al}_2\text{O}_3$ catalyst. MWCNTs with outer diameters of <8 nm, 30–50 nm and >50 nm were designated as MWCNTs8, MWCNTs30, MWCNTs50, respectively. According to the contained oxygen contents other MWCNTs with outer diameters of 10–20 nm were designated as MWCNTs-O(1.52%), MWCNTs-O(2.66%) and MWCNTs-O(7.58%), respectively.

The diameters of MWCNTs were determined by TEM. The carbon and oxygen contents were determined by X-ray photoelectron spectroscopy (ESCALab220i–XL electron spectrometer from VG Sci-

Table 1
Properties of diuron and dichlobenil.

| Properties | Diuron | Dichlobenil |
|--|---|---|
| Chemical formula | $\text{C}_9\text{H}_{10}\text{Cl}_2\text{N}_2\text{O}$ | $\text{C}_7\text{H}_3\text{Cl}_2\text{N}$ |
| Chemical structure |  |  |
| Molecular weight (g/mol) | 233.09 | 172.02 |
| Molecular volume (cm^3/mol) | 170.1 | 122.4 |
| Molecular surface area (nm^2) | 2.19 | 1.423 |
| Density (cm^3/g) | 1.1786 | 1.3 |
| Dipolar moment (Debyes) | 7.55 | 5.54 |
| Water solubility (mg L^{-1} , 20°C) | 40 | 18 |
| $\log K_{ow}$ | 2.85 | 2.74 |

entific) using 300W AlK α radiation under the base pressure of about 3×10^{-9} mbar. The surface area, pore volume and micropore were measured by nitrogen gas adsorption and desorption at 77 K with ASAP2020 accelerated surface area and porosimetry systems (Micromeritics Instrument Corporation), and then calculated by multi-point BET, BJH, and DR methods. The structural properties of MWCNTs are shown in Table 2. Preliminary experiments indicated that impurities of Pb^{2+} , diuron and dichlobenil in all MWCNTs were below the detection limits.

2.3. Batch adsorption

Briefly, 40 ml of glass tube sealed with Teflon-lined screw-caps was used as batch reactors. 5 mg of MWCNTs and 35 ml of diuron/dichlobenil solution at various concentrations (~ 0.6 – 22 mg L^{-1} of diuron and ~ 0.6 – 13 mg L^{-1} of dichlobenil) were utilized for all adsorption experiments. A mixture of 0.01 M NaNO_3 and 0.1 g/L NaN_3 was used as background solution. Reactors filled with MWCNTs and solutions were shaken at 100 rpm and $20 \pm 0.5^\circ\text{C}$ in a shaker (HZQ-F160) for 2 d at pH 6 (preliminary sorption studies indicated that apparent equilibration was reached <2 d). The pH of adsorbent suspension was adjusted to 6.0 ± 0.1 by drop wise addition of 0.1 M HNO_3 or 0.1 M NaOH at the beginning of reaction and remained constantly at the end of the adsorption. After centrifugation at $2000 \times g$ for 20 min, all glass tubes were placed vertically to stand for 24 h to ensure complete separation of aqueous phase from MWCNTs at $20 \pm 0.5^\circ\text{C}$ for diuron and dichlobenil. Supernatants were withdrawn and final concentrations of diuron and dichlobenil were determined by HPLC. After adsorption the suspension was filtered through a Millipore 0.25- μm hydrophilic polyethersulfone membrane and final Pb^{2+} concentrations remained in the supernatant were determined using ICP-AES (Perkin–Elmer).

Experimental recoveries of batch equilibrium experiments were evaluated without MWCNTs. Total recovery of each adsorbate was >97%. Therefore, the adsorbed diuron, dichlobenil, and Pb^{2+} by MWCNTs were directly calculated by mass differences between their initial and final concentrations.

Table 2
Selected structural properties of MWCNTs.

| MWCNTs | Outer diameter (nm) | C (%) | O (atom %) | Surface area (SA) ($\text{m}^2 \text{g}^{-1}$) | | | | |
|------------------|---------------------|-------|------------|--|----------------------|--------------------|--|---|
| | | | | BET SA | t-Plot micro-pore SA | t-Plot external SA | V_{meso} (cc g^{-1}) | V_{micro} (cc g^{-1}) |
| MWCNTs 8 | <8 | 97.9 | 2.1 | 558.15 | 67.33 | 490.81 | 1.62 | 0.117 |
| MWCNTs30 | 30–50 | 99.17 | 0.83 | 83.14 | 9.52 | 74.62 | 0.296 | 0.019 |
| MWCNTs50 | >50 | 98.75 | 1.25 | 60.83 | 5.73 | 55.1 | 0.158 | 0.015 |
| MWCNTs-O (1.52%) | 10–20 | 98.48 | 1.52 | 159.35 | 13.1 | 146.25 | 0.575 | 0.032 |
| MWCNTs-O (2.66%) | 10–20 | 97.34 | 2.66 | 156.52 | 15.4 | 141.12 | 0.521 | 0.032 |
| MWCNTs-O (7.58%) | 10–20 | 92.42 | 7.58 | 161.73 | 21.68 | 140.05 | 0.512 | 0.032 |

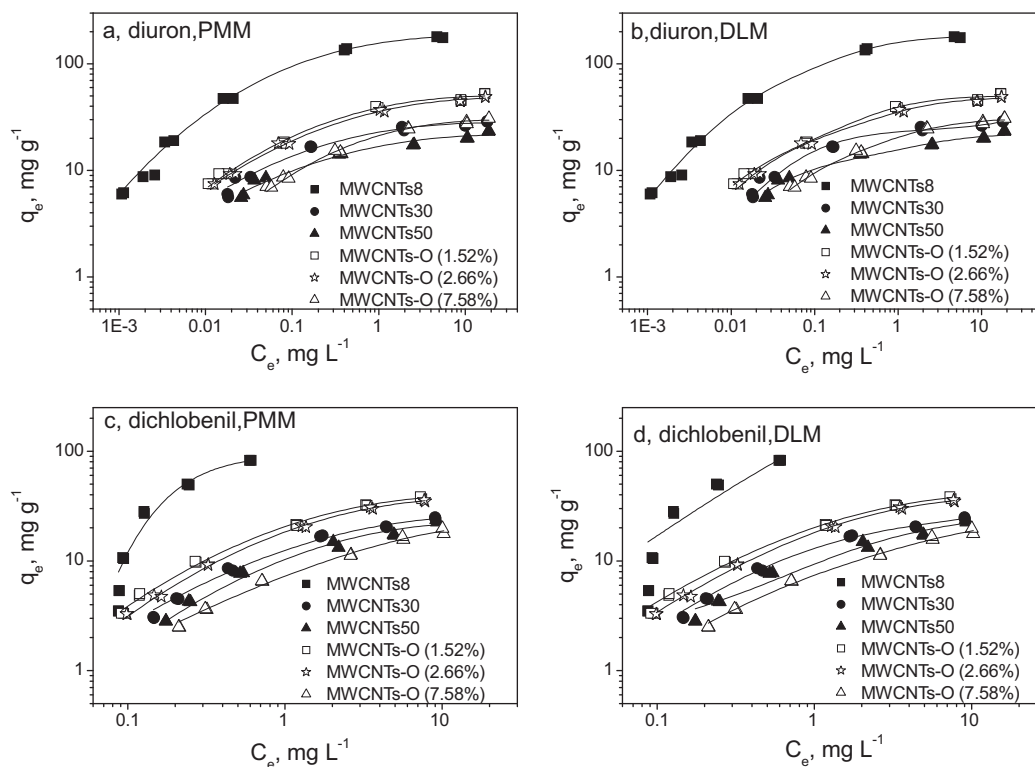


Fig. 1. Adsorption of diuron and dichlobenil on MWCNTs.

Table 3

Nonlinear sorption model.

| Model | Equation | Capacity term ^a |
|---------------|--|--|
| Polanyi–Manes | $q_e = Q^0 \text{EXP}(a(\epsilon_{sw}/V_s)^b) \epsilon_{sw} = RT \ln(C_s/C_e)$ | ϵ_{sw} [kJ/mol], effective adsorption potential; V_s [cm ³ mol ⁻¹], molar volume of solute; a [(cm ³) ^{b+1} (kg) ^{-b}] and b , fitting parameters; R [8.314×10^{-3} kJ (mol K) ⁻¹], universal gas constant; T [K], absolute temperature potential |
| Dual Langmuir | $q_e = q_{m1} b_1 C_e / (1 + b_1 C_e) + q_{m2} b_2 C_e / (1 + b_2 C_e)$ | q_{m1} [mg g ⁻¹] and q_{m2} [mg g ⁻¹], sorbed capacity of site populations 1 and 2, respectively; b_1 [L mg ⁻¹] and b_2 [L mg ⁻¹], affinity coefficient of site populations 1 and 2, respectively |

^a q_e [mg g⁻¹], equilibrium sorbed concentration; C_e [mg L⁻¹], equilibrium solution phase concentration; Q^0 [mg g⁻¹], adsorbed amount; C_s [mg L⁻¹], aqueous water solubility.

2.4. Analyses of diuron and dichlobenil

The concentrations of diuron and dichlobenil in equilibrium solutions were determined using a HPLC (Agilent Technologies 1200) equipped with a reversed-phase C₁₈ column (5 μ m, 4.6 mm \times 200 mm) and an UV–visible spectrophotometer (UV–visible HP 8452 A) at 252 nm for diuron and 238 nm for dichlobenil. The mobile phase was acetonitrile/water (50/50, volume ratio) for diuron, and methanol/water (65/35, volume ratio) for dichlobenil, with a flow rate of 1.0 mL min⁻¹. Detection limit of this method for diuron and dichlobenil was found to be \sim 10 ppb.

2.5. Fourier transform infrared micro-spectroscopic measurements

Fourier transform infrared micro-spectroscopic (μ -FTIR) spectra were recorded on NICOLET iN 10 MX (Thermo Scientific). Samples for μ -FTIR analysis were prepared with identical conditions to that used in the sorption experiments. MWCNTs, diuron- or dichlobenil-adsorbed MWCNTs were washed with above mentioned background solution and air-dried overnight. Micro-samples were pressed on a diamond bracket and μ -FTIR spectra

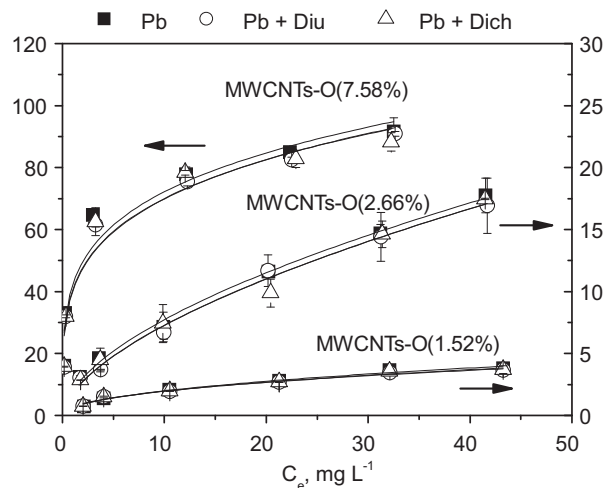


Fig. 2. Adsorption of lead to MWCNTs-O in the absence or presence of diuron or dichlobenil.

Table 4

Results of Polanyi–Manes model fitting to the adsorption isotherms of diuron and dichlobenil on MWCNTs.

| MWCNTs | Q^0 | a | b | Q_{SA} (mg m ⁻²) | S C | MWSE | R^2 |
|--------------------|---------------|-------------------|-------------|--------------------------------|--------------------------|--------------------|-------|
| Diuron | | | | | | | |
| MWCNTs8 | 182.72 ± 2.32 | -964.89 ± 237.31 | 2.98 ± 0.11 | 0.33 ± 0.03 | 1.85 ± 0.02 ^a | 0.02 ^b | 0.992 |
| MWCNTs30 | 27.32 ± 0.48 | -1181.51 ± 830.09 | 2.59 ± 0.46 | 0.34 ± 0.01 | 1.86 ± 0.03 ^a | 0.009 ^b | 0.996 |
| MWCNTs50 | 23.43 ± 1.15 | -243.39 ± 311.30 | 2.34 ± 0.55 | 0.38 ± 0.02 | 2.18 ± 0.11 ^a | 0.006 ^b | 0.986 |
| MWCNTs-O(1.52%) | 50.34 ± 1.02 | -422.35 ± 209.52 | 2.51 ± 0.22 | 0.32 ± 0.01 | 1.79 ± 0.04 ^a | 0.01 ^b | 0.974 |
| MWCNTs-O(2.66%) | 48.02 ± 1.08 | -293.26 ± 148.56 | 2.34 ± 0.22 | 0.31 ± 0.07 | 1.74 ± 0.04 ^a | 0.002 ^b | 0.996 |
| MWCNTs-O(7.58%) | 29.82 ± 1.02 | -613.42 ± 625.16 | 2.55 ± 0.41 | 0.18 ± 0.06 | 1.04 ± 0.03 ^a | 0.002 ^b | 0.997 |
| Dichlobenil | | | | | | | |
| MWCNTs8 | 96.30 ± 15.70 | -2.35E6 ± 1.90E5 | 6.15 ± 3.49 | 0.17 ± 0.03 | 0.86 ± 0.14 | 0.064 | 0.986 |
| MWCNTs30 | 24.60 ± 0.65 | -340.78 ± 166.78 | 2.20 ± 0.18 | 0.30 ± 0.01 | 1.48 ± 0.04 | 0.002 | 0.997 |
| MWCNTs50 | 22.15 ± 3.35 | -152.92 ± 94.71 | 2.18 ± 0.27 | 0.36 ± 0.06 | 1.81 ± 0.27 | 0.009 | 0.988 |
| MWCNTs-O(1.52%) | 39.35 ± 3.78 | -189.17 ± 68.91 | 2.31 ± 0.17 | 0.25 ± 0.02 | 1.23 ± 0.12 | 0.004 | 0.996 |
| MWCNTs-O(2.66%) | 37.16 ± 3.76 | -116.76 ± 21.66 | 2.07 ± 0.09 | 0.24 ± 0.02 | 1.18 ± 0.12 | 0.002 | 0.995 |
| MWCNTs-O(7.58%) | 23.46 ± 1.38 | -86.18 ± 32.83 | 1.60 ± 0.23 | 0.15 ± 0.01 | 0.72 ± 0.05 | 0.004 | 0.999 |

^a Is surface coverage.^b MWSE is mean weighted square error, equal to $1/\nu \sum [(q_{\text{measured}} - q_{\text{model}})^2 / q_{\text{measured}}^2]$, where ν is the amount of freedom; $\nu = N - 3$ for PMM, and $\nu = N - 4$ for DLM.

were measured. FTIR spectra of MWCNTs are the average of 120 accumulated scans using a nominal resolution of 16 cm⁻¹ due to very weak signals of MWCNTs, while spectra of pure diuron and dichlobenil are the average of 64 accumulated scans using a nominal resolution of 4 cm⁻¹.

2.6. X-ray absorption spectroscopic measurements and data analyses

X-ray absorption spectroscopic (XAS) spectra at Pb L_{III}-edge were obtained at 4W1B beamline of Beijing Synchrotron Radiation Facility using a Si (1 1 1) double crystal monochromator. Electron beam energy was 2.2 GeV with a storage ring beam current of 80 mA. Data analyses were performed using WinXAS2.1 following background correction and normalization, together with cubic spline, Fourier transformed, reverse Fourier transformed and EXAFS fittings. In the fitting procedure, the coordination number was fixed for the reference compounds, while the Debye–Waller factor was fixed for samples. Phase shifts and backscattering amplitudes were obtained from theoretical calculation using FEFF 7.0.

3. Results and discussion

3.1. Characterization of MWCNTs

Table 2 shows the selected structural properties of MWCNTs. Surface area and pore volume decreased in order of MWCNTs8 > MWCNTs-O(1.52%) ≈ MWCNTs-O(2.66%) > MWCNTs-O(7.58%) > MWCNTs30 > MWCNTs50. Among

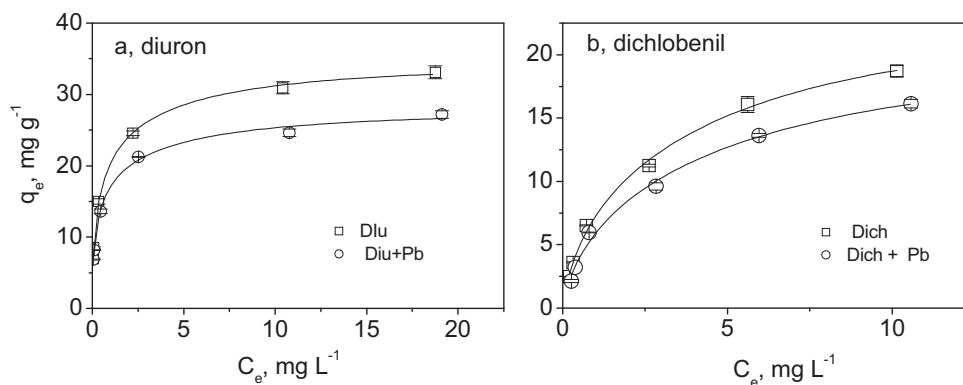
them, MWCNTs-O(1.52%), MWCNTs-O(2.66%) and MWCNTs-O(7.58%) have different oxygen contents given in the parenthesis, but have same outer diameters and surface areas.

3.2. Adsorption of diuron and dichlobenil

Adsorption isotherms of diuron and dichlobenil on the MWCNTs are depicted in Fig. 1. Polanyi–Manes and Dual Langmuir models (Table 3) were applied to fit the adsorption data. The former fit all the adsorption isotherms well with the lowest MWSE (Table 4), and the later fit the adsorption isotherms well in most of cases with the exception of MWCNTs8 (data not shown). Hence the following discussion was only based on the adsorption parameters of Polanyi–Manes model fitting.

The results suggested that the adsorption of diuron and dichlobenil increased with increasing surface areas and pore volumes of MWCNTs. MWCNTs8 had the largest adsorption amount for both herbicides because MWCNTs8 has the largest surface area and pore volume. MWCNTs-O(1.52%) and MWCNTs-O(2.66%) have significantly larger Q^0 than that of MWCNTs-O(7.58%), implying that an increase of oxygen content of MWCNTs decreased the adsorption due to deprotonation of carboxylic groups at pH 6 [28], hence adsorption of water is more energetically favorable to the adsorption of diuron and dichlobenil.

The Q_{SA} values were referred to as the normalized Q^0 by the surface areas of respective MWCNTs. Of Q_{SA} , MWCNTs50 has the largest Q_{SA} for both diuron and dichlobenil, although MWCNTs50 has the lowest adsorbed amount of diuron and dichlobenil (Table 4). We take Q_{SA} of MWCNTs50 for diuron (0.38 mg m⁻²)

**Fig. 3.** Effects of lead on the adsorption of diuron and dichlobenil by MWCNTs-O(7.58%).

an example, which was larger than that of activated carbon (0.36 mg m^{-2}), wheat carbon (0.11 mg m^{-2}) and granular activated carbon (0.27 mg m^{-2}), respectively, but smaller than that of activated carbon fiber (0.39 mg m^{-2}) and activated carbon cloth (0.41 mg m^{-2}), respectively [35,36].

The values of Q_{SA} and surface coverage (SC) of diuron are larger than that of dichlobenil, although the surface area, molecular volume and water solubility of dichlobenil are smaller. This discrepancy can partly be ascribed to greater van der Waals interactions for diuron than for dichlobenil due to the relatively larger dipolar moment [36]. These data show that the surface coverage of both herbicides is larger than 1, suggesting that the adsorption of both on MWCNTs was multilayer.

Because MWCNTs-O(1.52%), MWCNTs-O(2.66%), and MWCNTs-O(7.58%) have quite similar diameters and surface areas, but contain different oxygen contents, therefore we choose these MWCNTs to compare the effects of oxygen contents and lead on the adsorption of diuron and dichlobenil below.

3.3. Adsorption of lead

According to the speciation diagrams (Fig. A1), lead is mainly present as Pb^{2+} at pH 6, which accounts for 98% of total lead and PbOH^+ accounts for 2%. The adsorption isotherms of Pb^{2+} onto MWCNTs fit Freundlich equation well (Fig. 2). It is clearly indicated that the adsorption capacity of MWCNTs-O(1.52%) is only 3.79 mg g^{-1} at an equilibrium concentration of 32.54 mg L^{-1} for Pb^{2+} , while the adsorption capacities of MWCNTs-O(2.66%) and MWCNTs-O(7.58%) are 17.75 mg g^{-1} and 91.67 mg g^{-1} at the same equilibrium concentrations of Pb^{2+} . These data implied that the surface O-containing groups improved the ion-exchange capabilities of MWCNTs, and thus made Pb^{2+} adsorption increase accordingly. The underlying mechanisms of increased adsorption of lead by surface O-containing groups can be ascribed to “chemisorption” or chemicomplexation [11]. The dramatically increase of adsorption capacities of MWCNTs-O(7.58%) indicated that inner-sphere or outer-sphere complexes of Pb^{2+} are assumed to be formed on the surface of MWCNTs, which will be discussed in the XAS measurements.

It should be pointed out that the addition of 4 mg L^{-1} diuron or dichlobenil had little effect on the adsorption of Pb^{2+} for the tested MWCNTs (Fig. 2).

3.4. Adsorption of diuron and dichlobenil as affected by lead

To evaluate the effect of Pb^{2+} on the adsorption of diuron and dichlobenil, 50 mg L^{-1} of Pb^{2+} was simultaneously adsorbed with diuron and dichlobenil because this Pb concentration corresponds to the second level of Environmental Quality Standard for lead (250 mg kg^{-1}) in Chinese soils if all Pb^{2+} were adsorbed.

The co-adsorption of Pb^{2+} with diuron or dichlobenil indicated that Pb^{2+} significantly suppressed the adsorption of diuron or dichlobenil on MWCNTs-O(7.58%) (Fig. 3), and had little effect on the adsorption of herbicides onto MWCNTs-O(2.66%) and MWCNTs-O(1.52%) (Fig. A2). The Pb^{2+} suppression effect on the adsorption of diuron or dichlobenil was expressed as $(K_d^2 - K_d^1)/K_d^1$, where K_d^2 and K_d^1 represent the distribution coefficients of diuron or dichlobenil in the presence and absence of Pb^{2+} , respectively. The presence of Pb^{2+} decreased diuron adsorption onto MWCNTs-O(7.58%) by $\sim 10\text{--}30\%$ and decreased dichlobenil sorption onto MWCNTs-O(7.58%) by $\sim 15\text{--}30\%$, respectively.

In order to explore the underlying mechanisms why Pb^{2+} suppressed the adsorption of diuron and dichlobenil we used μ -FTIR and XAS study to provide an insight to the relevant mechanisms.

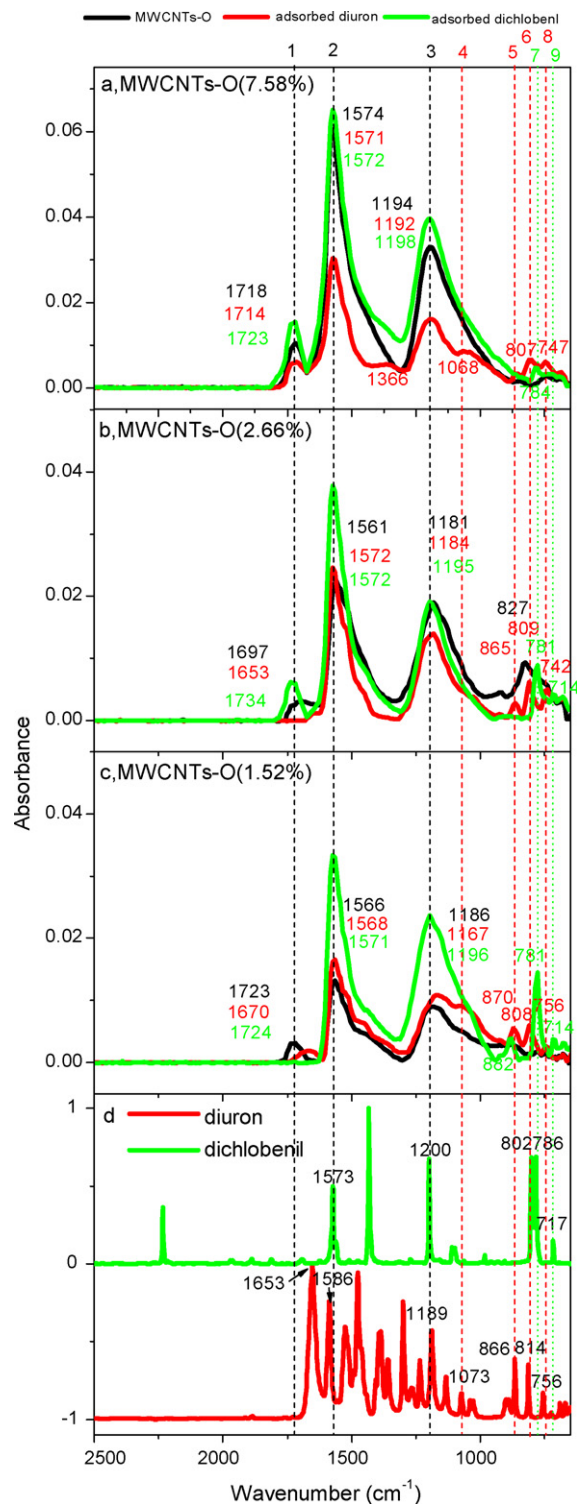


Fig. 4. μ -FTIR spectra of MWCNTs-O(7.58%) (a), MWCNTs-O(2.66%) (b), and MWCNTs-O(1.52%) (c) without and with diuron or dichlobenil adsorbed, and pure diuron or dichlobenil (d).

3.5. μ -FTIR analysis

To reveal the adsorption sites and verify the existence of hydrogen bonding of diuron and dichlobenil, a μ -FTIR study was performed. The μ -FTIR spectra of MWCNTs-O, diu-MWCNTs-O, and Dich-MWCNTs-O in the frequency range of $650\text{--}2500 \text{ cm}^{-1}$ are shown in Fig. 4. As can be seen in Fig. 4a–c (black lines) the peaks at

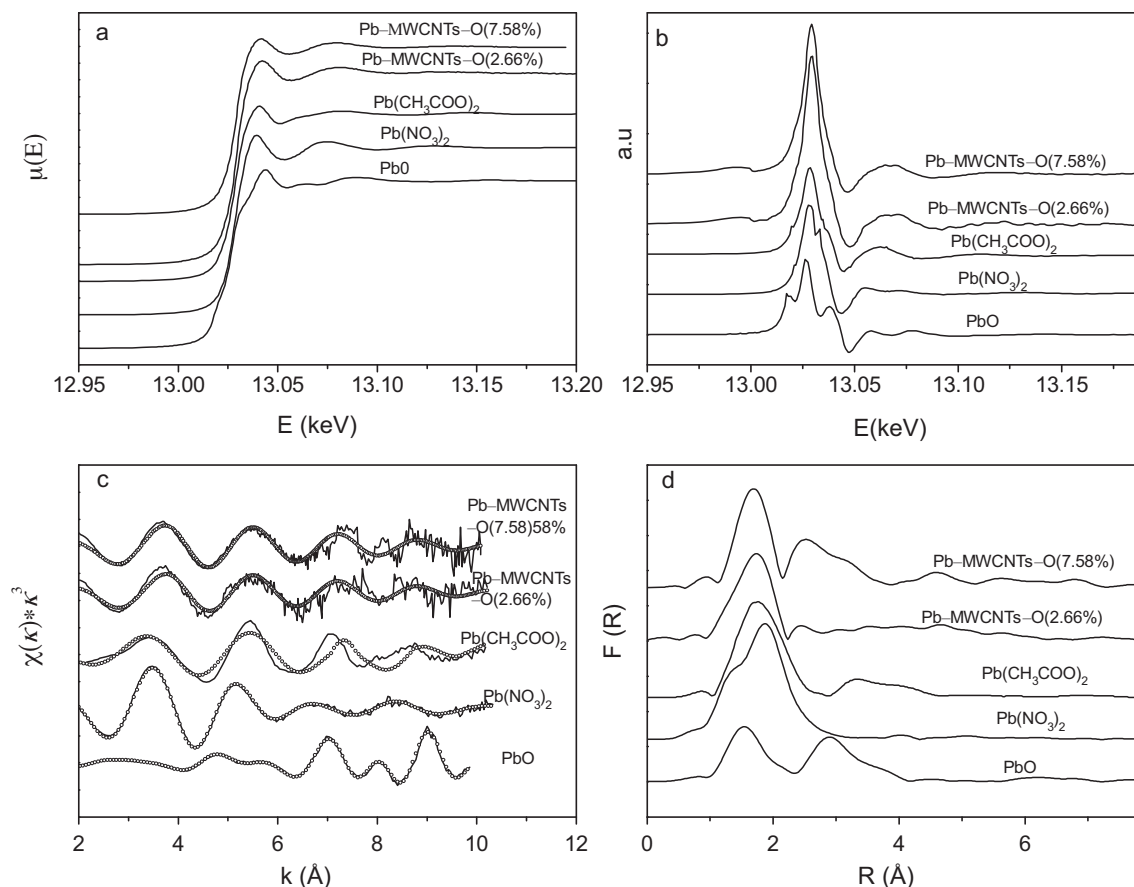


Fig. 5. Normalized XANES spectra (a), corresponding first derivatives (b), EXAFS spectra (χ -function) (c), and Fourier transformation of EXAFS spectra (d) of Pb^{2+} -MWCNTs-O(7.58%) and Pb^{2+} -MWCNTs-O(2.66%).

$\sim 1194\text{ cm}^{-1}$ can be assigned to C–O stretching vibration [37], the peaks at $\sim 1574\text{ cm}^{-1}$ for –COO– to asymmetric stretching vibration of carboxylic bond [11,18,38,39], the peaks at $\sim 1718\text{ cm}^{-1}$ to C=O stretch of keto or carboxyl groups [11,38].

For diuron (Fig. 4d, red line), the most intense bands were carbonyl peak at $\sim 1653\text{ cm}^{-1}$ and benzene ring stretching at ~ 1525 , ~ 1476 , and $\sim 1394\text{ cm}^{-1}$. Other absorption bands are located at 1586 cm^{-1} due to C=C stretching vibration [1,40], and 1189 cm^{-1} due to C–H in-plane bending vibration of benzene ring, respectively. Peaks at ~ 816 , ~ 866 and $\sim 756\text{ cm}^{-1}$ are assigned to mainly C–H out-of plane bending vibration of benzene ring, and partly C–Cl stretching vibration. For dichlobenil (Fig. 4d, green line), peak at $\sim 1573\text{ cm}^{-1}$ is assigned to C=C stretching vibration, peak at $\sim 1433\text{ cm}^{-1}$ to benzene ring stretching, and $\sim 1200\text{ cm}^{-1}$ to in-plane bending vibration of benzene ring, peaks at ~ 802 , ~ 786 , $\sim 717\text{ cm}^{-1}$ mainly to C–H out-of plane bending vibration of benzene ring, and partly C–Cl stretching vibration.

After diuron was adsorbed to MWCNTs-O(7.58%), MWCNTs-O(2.66%) and MWCNTs-O(1.52%), new peaks appeared at $\sim 807\text{ cm}^{-1}$, $\sim 747\text{ cm}^{-1}$ (Fig. 4a, red line), 809 cm^{-1} , 742 cm^{-1} (Fig. 4b, red line) and $\sim 870\text{ cm}^{-1}$, 808 cm^{-1} (Fig. 4c, red line), respectively, which were assigned to C–H out-of plane bending vibration of benzene ring of diuron. The C–O stretching vibration peaks at $\sim 1194\text{ cm}^{-1}$ (Fig. 4a, black line), 1181 cm^{-1} (Fig. 4b, black line) and 1186 cm^{-1} (Fig. 4c, black line) [1,40] were shifted to $\sim 1192\text{ cm}^{-1}$ (Fig. 4a, red line), 1184 cm^{-1} (Fig. 4b, red line) and 1167 cm^{-1} (Fig. 4c, red line), respectively, which can be assigned to C–H in-plane bending vibration of benzene ring at 1189 cm^{-1} of diuron and the interaction between the C–O and the benzene ring. The –COO– asymmetric stretching peaks at $\sim 1574\text{ cm}^{-1}$

(Fig. 4a, black line), 1561 cm^{-1} (Fig. 4b, black line), 1566 cm^{-1} (Fig. 4c, black line) [1,40] were shifted to 1571 cm^{-1} (Fig. 4a, red line), 1572 cm^{-1} (Fig. 4b, red line) and 1568 cm^{-1} (Fig. 4c, red line), which were assigned to the C=C stretching vibration at 1586 cm^{-1} of diuron and the interaction between the –COO– and the benzene ring. The C=O stretch peaks at $\sim 1718\text{ cm}^{-1}$ (Fig. 4a, black line), 1697 cm^{-1} (Fig. 4b, black line), 1723 cm^{-1} (Fig. 4c, black line) [1,40] were shifted to $\sim 1714\text{ cm}^{-1}$ (Fig. 4a, red line), 1653 cm^{-1} (Fig. 4b, red line), 1670 cm^{-1} (Fig. 4c, red line). These new appeared peaks and the band shifts on MWCNTs-O(7.58%) suggested that diuron was partly adsorbed on surface of MWCNTs-O(7.58%) by hydrogen bonding through the C=O, or –COO– groups.

After dichlobenil was adsorbed, new peaks at $\sim 784\text{ cm}^{-1}$ appeared on MWCNTs-O(7.58%) (Fig. 4a, green lines), $\sim 784\text{ cm}^{-1}$, and 714 cm^{-1} on MWCNTs-O(2.66%) (Fig. 4b, green lines), 882 cm^{-1} , 781 cm^{-1} , and 714 cm^{-1} on MWCNTs-O(1.52%) (Fig. 4c, green lines), which were assigned to C–H out-of plane bending vibration of benzene ring of dichlobenil. The C–O stretching vibration peaks at $\sim 1194\text{ cm}^{-1}$ (Fig. 4a, black line), 1181 cm^{-1} (Fig. 4b, black line) and 1186 cm^{-1} (Fig. 4c, black line) were shifted to 1198 cm^{-1} (Fig. 4a, green line), 1196 cm^{-1} (Fig. 4b, green line), and 1196 cm^{-1} (Fig. 4c, green line) for MWCNTs-O(7.58%), MWCNTs-O(2.66%) and MWCNTs-O(1.52%), respectively, which were assigned to the in-plane bending vibration of benzene ring, at 1200 cm^{-1} of dichlobenil and the interaction between C–O and benzene ring. The –COO– asymmetric stretching vibration peaks at $\sim 1574\text{ cm}^{-1}$ (Fig. 4a, black line), 1561 cm^{-1} (Fig. 4b, black line), 1566 cm^{-1} (Fig. 4c, black line) were shifted to 1572 cm^{-1} (Fig. 4a, green line), 1572 cm^{-1} (Fig. 4b, green line) and 1571 cm^{-1} (Fig. 4c, green line) for MWCNTs-O(7.58%), MWCNTs-O(2.66%)

and MWCNTs-O(1.52%), respectively, which were assigned to C=C stretching vibration at 1573 cm^{-1} and interaction of $-\text{COO}-$ and benzene ring. The C=O stretch at $\sim 1718\text{ cm}^{-1}$ (Fig. 4a, black line), 1697 cm^{-1} (Fig. 4b, black line), was shifted to 1723 cm^{-1} (Fig. 4a, green line), 1734 cm^{-1} (Fig. 4b, green line), for MWCNTs-O(7.58%), and MWCNTs-O(2.66%), respectively, which were assigned to interaction of dichlobenil and MWCNTs-O.

Considering the high electronegativity of O atom within C=O groups and the presence of H atom from O–H bond of MWCNTs, it was assumed that hydrogen bonding is the most probable reaction mode between diuron or dichlobenil with MWCNTs-O.

3.6. XAS analysis

XAS was used to identify the surface complexation and to obtain the coordination environment of Pb^{2+} adsorbed onto MWCNTs. Identification of such complex formation provides an insight into the suppression mechanism of diuron and dichlobenil adsorption by Pb^{2+} .

Pb L_{III} XANES spectra are quite sensitive to local atomic structure of the first few neighbor atom shells [41]. Distinct differences in near-edge structure can facilitate discrimination between model compounds and adsorbed samples, in which Pb is coordinated in different environments. The XANES (Fig. 5a) of Pb^{2+} showed a distinct difference shoulder around 13.00–13.05 keV and 13.05–13.10 keV region among PbO , $\text{Pb}(\text{NO}_3)_2$, $\text{Pb}(\text{CH}_3\text{COO})_2$, and Pb^{2+} -MWCNTs-O(7.58%) and Pb^{2+} -MWCNTs-O(2.66%). The similarities in XANES spectra between Pb^{2+} -MWCNTs-O(7.58%), Pb^{2+} -MWCNTs-O(2.66%) and $\text{Pb}(\text{CH}_3\text{COO})_2$ suggested that the coordination environment of Pb in those compounds was similar. Roe et al. [42] proposed the presence of an intense peak at $\sim 40\text{ eV}$ above the first sharp peak in the first derivative spectra of XANES for Pb as an indicator of outer-sphere complexation. However, there was no such feature at this energy level in the first derivative spectra of XANES for Pb^{2+} -MWCNTs-O(7.58%) and Pb^{2+} -MWCNTs-O(2.66%) (Fig. 5b).

The k^3 -weighted EXAFS spectra for Pb^{2+} -MWCNTs-O(7.58%) and Cu -MWCNTs-O(2.66%) and their corresponding radial structural functions (RSF) derived from Fourier transformation are presented in Fig. 5c and d. A good agreement was obtained between the spectra of Pb^{2+} -MWCNTs-O(7.58%) and Pb^{2+} -MWCNTs-O(2.66%) and that of $\text{Pb}(\text{CH}_3\text{COO})_2$ among the first three oscillations at 3.7, 5.6 and 7.1 Å, which constitute a good fingerprint of $\text{Pb}(\text{CH}_3\text{COO})_2$ (Fig. 5c), and indicate Pb^{2+} coordination on MWCNTs-O(7.58%) and MWCNTs-O(2.66%) through carboxylic moieties. Fig. 5d shows a broad peak centered at $\sim 1.7\text{ Å}$ for Pb^{2+} -MWCNTs-O(7.58%), Pb^{2+} -MWCNTs-O(2.66%) and $\text{Pb}(\text{CH}_3\text{COO})_2$, which results from backscattering in the first coordination shell of Pb atoms. The fitting of this peak leads to 1.8 oxygen atoms at 2.38 Å for Pb^{2+} -MWCNTs-O(7.58%) and 1.8 oxygen atoms at 2.37 Å for Pb^{2+} -MWCNTs-O(2.66%). These results are similar to that of Dupont et al. [43]. The coordination number was particularly low as expected because of the highly structural disorder of Pb coordination shells. The L_{III} -edge XANES spectra (Fig. 5a), EXAFS functions (Fig. 5c) and corresponding radial structure function (Fig. 5d) appeared to be very similar for Pb^{2+} -MWCNTs-O(7.58%), Pb^{2+} -MWCNTs-O(2.66%) and $\text{Pb}(\text{CH}_3\text{COO})_2$, which indicated Pb coordination on MWCNTs-O(7.58%) and MWCNTs-O(2.66%) mostly through carboxylic moieties.

4. Conclusion

The adsorption of diuron and dichlobenil was closely correlated with surface areas and micropore volumes of MWCNTs. Of them, MWCNTs50 had the largest Q_{SA} , although the adsorbed diuron and

dichlobenil were lower, implying that MWCNTs50 had the highest adsorption capacity. An increase in the oxygen contents decreased the adsorption of diuron and dichlobenil, while increased the adsorption of lead for MWCNTs with outer diameter of 10–20 nm.

The presence of Pb^{2+} decreased the adsorption of diuron and dichlobenil. Two mechanisms may be involved. Complexation of Pb^{2+} with carboxylic groups and hydrated lead cation occupy part of surface of MWCNTs-O. The metal cation hydration shells may intrude or shield the hydrophobic and hydrophilic sites of MWCNTs, leading to the inhibition of adsorption of diuron and dichlobenil around the metal-complexed moieties.

Acknowledgments

This work was funded by the National Natural Science Foundation of China (grant number: 41071308). Dr. Weng Shifu, College of Chemistry and Molecular Engineering, Peking University, was highly appreciated for his constructive discussion on FTIR data.

Appendix A. Supplementary data

Supplementary data associated with this article can be found, in the online version, at doi:10.1016/j.jhazmat.2011.01.095.

References

- [1] S. Armenta, G. Quinaas, A. Morales, S. Garrigues, M.D.L. Guardiaj, FTIR approaches for diuron determination in commercial pesticide formulations, *J. Agric. Food. Chem.* 53 (2005) 5842–5847.
- [2] C. Cox, Herbicide factsheet: dichlobenil, *J. Pestic. Reform.* 17 (1997) 14–20.
- [3] J.H. Montgomery, *Agrochemicals Desk Reference*, Lewis Publishers, Chelsea, MI, 1993, p. 625.
- [4] L. Clausen, F. Larsen, H.J. Albrechtsen, Sorption of the herbicide dichlobenil and the metabolite 2,6-dichlorobenzamide on soils and aquifer sediments, *Environ. Sci. Technol.* 38 (2004) 4510–4518.
- [5] A. Newman, Ranking pesticides by environmental impact, *Environ. Sci. Technol.* 29 (1995) 324A–326A.
- [6] P. Li, X. Wang, G. Allinsonb, X. Li, X. Xiong, Risk assessment of heavy metals in soil previously irrigated with industrial wastewater in Shenyang, China, *J. Hazard. Mater.* 161 (2009) 516–521.
- [7] P.W. Purdom, *Environmental Health*, Academic Press, New York, 1980.
- [8] Y.H. Li, S. Wang, J. Wei, X. Zhang, Z. Luan, D. Wu, B. Wei, Lead adsorption on carbon nanotubes, *Chem. Phys. Lett.* 357 (2002) 263–266.
- [9] Y.H. Li, J. Ding, Z.K. Luan, Z.C. Di, Y.F. Zhu, C.L. Xu, D.H. Wu, B.O. Wei, Competitive adsorption of Pb^{2+} , Cu^{2+} and Cd^{2+} ions from aqueous solutions by multiwalled carbon nanotubes, *Carbon* 41 (2003) 2787–2792.
- [10] Y.H. Li, Z. Di, J. Ding, D. Wu, Z. Luan, Y. Zhu, Adsorption thermodynamic, kinetic and desorption studies of Pb^{2+} on carbon nanotubes, *Water Res.* 39 (2005) 605–609.
- [11] X.K. Wang, G. Chen, W. Hu, A. Ding, D. Xu, X. Zhou, Sorption of $^{243}\text{Am}(\text{III})$ to multiwall carbon nanotubes, *Environ. Sci. Technol.* 39 (2005) 2856–2860.
- [12] J. Hu, C.L. Chen, X.X. Zhu, X.K. Wang, Removal of chromium from aqueous solution by using oxidized multiwalled carbon nanotubes, *J. Hazard. Mater.* 162 (2009) 1542–1550.
- [13] R.Q. Long, R.T. Yang, Carbon nanotubes as superior sorbent for dioxin removal, *J. Am. Chem. Soc.* 123 (2001) 2058–2059.
- [14] C. Lu, Y.L. Chung, K.F. Chang, Adsorption of trihalomethanes from water with carbon nanotubes, *Water Res.* 39 (2005) 1183–1189.
- [15] C.J.M. Chin, L.C. Shih, H.J. Tsai, T.K. Liu, Adsorption of o-xylene and p-xylene from water by SWCNTs, *Carbon* 45 (2007) 1254–1260.
- [16] M.S. Mauter, M. Elimelech, Environmental applications of carbon-based nanomaterials, *Environ. Sci. Technol.* 42 (2008) 5843–5859.
- [17] B. Fugetsu, S. Satoh, T. Shiba, T. Mizutani, Y. Lin, N. Terui, Y. Nodasaka, K. Sasa, K. Shimizu, T. Akasaka, M. Shindoh, K. Shibata, A. Yokoyama, M. Mori, K. Tanaka, Y. Sato, K. Tohji, S. Tanaka, N. Nishi, F. Watari, Caged multiwalled carbon nanotubes as the adsorbents for affinity-based elimination of ionic dyes, *Environ. Sci. Technol.* 38 (2004) 6890–6896.
- [18] X.M. Yan, B.Y. Shi, J.J. Lu, C.H. Feng, D.S. Wang, H.X. Tang, Adsorption and desorption of atrazine on carbon nanotubes, *J. Colloid Interface Sci.* 321 (2008) 30–38.
- [19] K. Yang, L.Z. Zhu, B.S. Xing, Adsorption of polycyclic aromatic hydrocarbons by carbon nanomaterials, *Environ. Sci. Technol.* 40 (2006) 1855–1861.
- [20] S. Gotovac, L. Song, H. Kanoh, K. Kaneko, Assenthy structure control of single wall carbon nanotubes with liquid phase naphthalene adsorption, *Colloids Surf. A* 300 (2007) 117–121.
- [21] K. Pyrzyńska, A. Stafiej, M. Biesaga, Sorption behavior of acidic herbicides on carbon nanotubes, *Microchim. Acta* 159 (2007) 293–298.

- [22] R.J. Chen, S. Bangsaruntip, K.A. Drouvalakis, N.W.S. Kam, M. Shim, Y.M. Li, W. Kim, P.J. Utz, H.J. Dai, Noncovalent functionalization of carbon nanotubes for highly specific electronic biosensors, *Proc. Natl. Acad. Sci. U.S.A.* 100 (2003) 4984–4989.
- [23] F. Balavoine, P. Schultz, C. Richard, V. Mallouh, T.W. Ebbesen, C. Mioskowski, Helical crystallization of proteins on carbon nanotubes: a first step towards the development of new biosensors, *Angew. Chem. Int. Ed.* 38 (1999) 1912–1915.
- [24] J. Zhang, J.K. Lee, Y. Wu, R.W. Murray, Photoluminescence and electronic interaction of anthracene derivatives adsorbed on sidewalls of single-walled carbon nanotubes, *Nano Lett.* 3 (2003) 403–407.
- [25] W. Chen, L. Duan, D.Q. Zhu, Adsorption of polar and nonpolar organic chemicals to carbon nanotubes, *Environ. Sci. Technol.* 41 (2007) 8295–8300.
- [26] W. Chen, L. Duan, L. Wang, D.Q. Zhu, Adsorption of hydroxyl and amino-substituted aromatics to carbon nanotubes, *Environ. Sci. Technol.* 42 (2008) 6862–6868.
- [27] D.H. Lin, B.S. Xing, Adsorption of phenolic compounds by carbon nanotubes: role of aromaticity and substitution of hydroxyl groups, *Environ. Sci. Technol.* 42 (2008) 7254–7259.
- [28] G.C. Chen, X.Q. Shan, Y.S. Wang, Z.G. Pei, X.E. Shen, B. Wen, G. Owens, Effects of copper, lead, and cadmium on the sorption and desorption of atrazine onto and from carbon nanotubes, *Environ. Sci. Technol.* 42 (2008) 8297–8302.
- [29] B. Pan, D. Lin, H. Mashayekhi, B.S. Xing, Adsorption and hysteresis of bisphenol A and 17 α -ethinyl estradiol on carbon nanomaterials, *Environ. Sci. Technol.* 42 (2008) 5280–5485.
- [30] H.J. Wang, A.L. Zhou, F. Peng, H. Yu, J. Yang, Mechanism study on adsorption of acidified multiwalled carbon nanotubes to Pb(II), *J. Colloid Interface Sci.* 316 (2007) 277–283.
- [31] J.Y. Dai, M.Q. Xu, J.P. Chen, X.P. Yang, Z.S. Ke, PCDD/F, PAH and heavy metals in the sewage sludge from six wastewater treatment plants in Beijing, China, *Chemosphere* 66 (2007) 353–361.
- [32] S. Dousset, A.R. Jacobson, J.B. Dessogne, N. Guichard, P.C. Baveye, F. Andreux, Facilitated transport of diuron and glyphosate in high copper vineyard soils, *Environ. Sci. Technol.* 41 (2007) 8056–8061.
- [33] Z.G. Pei, X.Q. Shan, B. Wen, B. He, T. Liu, Y.N. Xie, G. Owens, Sorption of anionic metsulfuron-methyl and cationic difenzoquat on peat and soil as affected by copper, *Environ. Sci. Technol.* 42 (2008) 6849–6854.
- [34] G.C. Chen, X.Q. Shan, Y.S. Wang, B. Wen, Z.G. Pei, Y.N. Xie, T. Liu, J.J. Pignatello, Adsorption of 2,4,6-trichlorophenol onto multi-walled carbon nanotubes as affected by Cu (II), *Water Res.* 43 (2009) 2409–2418.
- [35] Y. Yang, Y. Chun, G. Sheng, M. Huang, pH-Dependence of pesticide adsorption by wheat-residue-derived black carbon, *Langmuir* 20 (2004) 6736–6741.
- [36] M.V. López-Ramón, M.A. Fontecha-Cámara, M.A. Álvarez-Merino, C. Moreno-Castilla, Removal of diuron and amitrole from water under static and dynamic conditions using activated carbons in form of fibers, cloth, and grains, *Water Res.* 41 (2007) 2865–2870.
- [37] J. Peng, X.X. Qu, G.S. Wei, J.Q. Li, J.L. Qiao, The cutting of MWCNT using gamma radiation in the presence of dilute sulfuric acid, *Carbon* 42 (2004) 2735–2777.
- [38] S.D. Kim, J.W. Kim, J.S. Im, Y.H. Kim, Y.S. Lee, Oxidation of multiwalled carbon nanotubes by nitric acid, *J. Fluorine Chem.* 128 (2007) 60–64.
- [39] R.V. Hull, L. Li, Y. Xing, C.C. Chusuei, Pt nanoparticle binding on functionalized multiwalled carbon nanotubes, *Chem. Mater.* 18 (2006) 1780–1788.
- [40] D. Lin-Vien, N.B. Colthup, W.G. Fateley, J.G. Grasselli, *Infrared and Raman Characteristic Frequencies of Organic Molecules*, Academic Press, London, 1991.
- [41] D.G. Strawn, D.L. Sparks, The use of XAFS to distinguish between inner- and outer-sphere lead adsorption complexes on montmorillonite, *J. Colloid Interface Sci.* 216 (1999) 257–269.
- [42] A.L. Roe, F. Kim, J. Hayes, C. Chisholm-Brause, G.E. Brown Jr., G.A. Parks, K.O. Hodgson, J.O. Leckiel, In situ X-ray absorption study of lead ion surface complexes at the goethite–water interface, *Langmuir* 7 (1991) 367–373.
- [43] L. Dupont, E. Guillon, J. Bouanda, J. Dumonceau, M. Aplincourt, EXAFS and XANES studies of retention of copper and lead by a lignocellulosic biomaterial, *Environ. Sci. Technol.* 36 (2002) 5062–5066.